ELSEVIER

Contents lists available at ScienceDirect

Materials Today Communications

journal homepage: www.elsevier.com/locate/mtcomm



Deformation behavior of metallic glass composites and plasticity accommodation at microstructural length-scales



Vahid Hasannaeimi^a, Saideep Muskeri^a, Bharat Gwalani^{a,b}, Douglas C. Hofmann^c, Sundeep Mukherjee^{a,*}

- ^a Department of Materials Science and Engineering, University of North Texas, Denton, TX 76203, USA
- ^b Physical and Computational Sciences Directorate, Pacific Northwest National Laboratory, 902 Battelle Blvd, Richland WA, USA
- ^c NASA Jet Propulsion Laboratory, California Institute of Technology, 4800 Oak Grove Dr., Pasadena, CA 91109, USA

ARTICLE INFO

Keywords: Bulk metallic glass matrix composite Micro-pillar compression Mechanical properties TEM analysis

ABSTRACT

Bulk metallic glass matrix composites represent a unique microstructural design strategy for overcoming the strength/ductility trade-off in structural alloys. Site-specific mechanical behavior of a Ti-based bulk metallic glass composite was evaluated at microstructural length-scale. The micro-pillars on the amorphous matrix showed an average yield point of 1.9 GPa followed by serrated plastic deformation characteristic of shear banding. In contrast, micro-pillars on the crystalline dendritic phase showed a much lower yield strength of 0.72 GPa on average for the four different crystallographic orientations chosen, smooth plastic flow with no recognizable load burst, and stable strain-hardening after yield point. A number of micro-pillars were made at the interface between the glassy matrix and the crystalline dendrite. The mixed micro-pillars showed homogeneous deformation and greater plasticity which was attributed to their smaller stored elastic energy. Shear bands initiated in the amorphous matrix were arrested by the crystalline dendrite, which accommodated plasticity through slip bands and dislocations pile-ups. The interface remained intact after plastic deformation, with no observable signs of devitrification in the amorphous phase.

1. Introduction

Strength and ductility of metals are typically inversely correlated, where increase in strength by thermo-mechanical processing and microstructure modification leads to ductility reduction in most cases. However, high fracture toughness achieved by simultaneously increasing strength and total strain to failure remains a coveted goal in structural alloy design. Bulk metallic glass matrix composites (BMGMCs), consisting of in situ crystalline dendrites distributed uniformly in an amorphous matrix, represent a unique microstructural design strategy for achieving very high toughness while still retaining high strength [1]. Toughness values for some of these composites are among the highest reported for structural alloys ($K_{1C} > 100 \, \text{MPa} \, \text{m}^{1/2}$ 2), with greater than 10% total strain to failure [2-4]. Plastic deformation in monolithic amorphous alloys typically leads to flow localization in the form of shear bands, unabated movement of which leads to catastrophic failure [5]. In case of the metallic glass composites, the underlying mechanism for increase in fracture toughness is believed to be the deflection and blunting of crack tip at the ductile dendritic phase [6]. From a microstructural design approach, the spacing between ductile dendrite arms in BMGMCs should be less than the critical crack size required for fracture [7]. Consequently, single shear bands are arrested by the dendrites before they reach critical length. This results in the formation of multiple shear bands in BMGMCs under external loading and substantially enhances plasticity of the material as each shear band accommodates certain portion of the overall plastic deformation [8]. Since the load is still carried by the amorphous matrix, high strengths are still achievable, even with a significant volume fraction of dendrites. However, the contribution from each phase in accommodating plastic deformation as well as the response of the interface between amorphous matrix and crystalline dendrite is not well understood. Fundamental insights into phase-specific plastic flow at microstructural length-scales may pave the way for the development of next generation composites with ultra-high tough-

Here, we show the phase-specific deformation behavior of a Tibased metallic glass matrix composite. The stress–strain response was obtained for micro-pillars in the amorphous matrix and *in situ* crystalline dendrite concurrent with direct observation of their respective deformation behaviors inside a scanning electron microscope. Post-

E-mail address: sundeep.mukherjee@unt.edu (S. Mukherjee).

^{*} Corresponding author.

deformation analyses and high resolution transmission electron microscopy were utilized in understanding the role of the amorphous-crystalline interface in accommodation of plasticity and arrest of failure.

2. Materials and methods

An in situ bulk metallic glass matrix composite (BMGMC) of nominal composition $Ti_{48}Zr_{20}V_{12}Cu_5Be_{15}$ was chosen for this study [1]. The composite consisted of 53 vol% of amorphous phase with composition Ti₃₂Zr₂₅V₅Cu₁₀Be₂₈ and 47 vol% of dendritic body centered cubic (BCC) phase with composition Ti₆₆V₁₉Zr₁₄Cu₁. The surface of the specimen was polished to a mirror finish and ultrasonically cleaned with acetone and distilled water. Electron backscatter diffraction (EBSD) analysis was performed with FEI Nova Nano scanning electron microscope (SEM) to determine the micro-pillars orientation. Micro-pillars were fabricated on each phase as well as the phase boundaries using a dual beam Focused Ion Beam (FIB) in a SEM (FEI Nova 200) with diameters of 2 \pm 0.2 µm and aspect ratio (height/diameter) of 2.0–2.5. Ga-ion beam was used to mill the pillars in the FIB with a high current (30 keV and 3 nA) initially followed by gradual decrease to a value of 10 pA for the final milling. The taper angles for the pillars were found to be $\sim 2.0^{\circ}$ to 3.0° . The average diameter of each pillar was used for the calculation of engineering stress. At least 6 pillars were fabricated separately on the amorphous matrix, crystalline dendrite, and the interface between the two phases.

The micro-pillars were subjected to uniaxial compression inside the SEM chamber using Bruker PI88 SEM Pico-Indenter with a 500 mN load cell in displacement–control mode. All the pillars were compressed at a constant strain rate of $\sim 2.5 \times 10^{-4} \, \text{s}^{-1}$. A flat diamond tip with a diameter of 5 μ m was used for the compression tests. In order to capture discrete flow events during uniaxial compression, the data acquisition rate was set to the maximum value of 200 pts/sec. All the compression experiments were video-recorded at 0.1 frames/s along with synchronized load-displacement data (shown in supplementary videos). Using the pillar diameter and height, the load-displacement data were converted to engineering stress–strain curves. The morphology of the micro-pillars before and after compression were examined along with the images obtained *in situ* during the test.

3. Results

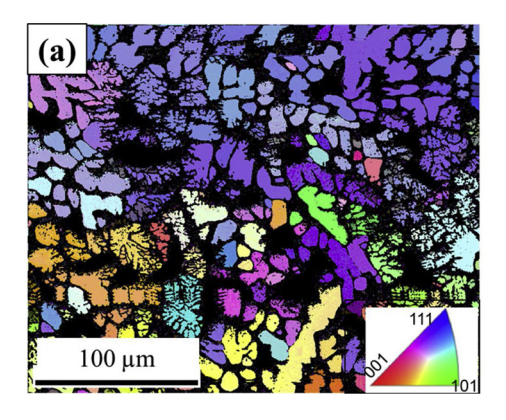
Electron backscatter diffraction (EBSD) inverse pole figure and image quality (IPF+IQ) map of the BMGMC is shown in Fig. 1a with the different crystallographic orientations for the dendritic phase. The metallic glass matrix was shown in black color due to the lack of backscatter signal from the amorphous structure. Micro-pillars on the dendritic phase were FIB-milled in the four different crystalline orientations of (213), (223), (307) and (507), which were in the largest volume fraction for the region chosen. Fig. 1b shows the SEM image of a

region containing a set of the micro-pillars in the crystalline dendrite and the amorphous matrix along with the pole figures of the micro-pillars in the dendritic phase. The point located in the center of the pole figures (circled in red) shows the chosen orientation for the compression studies.

The morphology of several representative micro-pillars on the amorphous matrix, crystalline dendrite, and the crystalline/amorphous interface before and after compression are shown in Fig. 2. The brighter contrast phase corresponds to the glassy matrix (Fig. 2a) while the darker phase corresponds to crystalline dendrite (Fig. 2b). Some of the micro-pillars consisted of a mixture of both crystalline and amorphous phases (Fig. 2c), while some were milled precisely at the crystalline/amorphous interface (Fig. 2d). The fully amorphous micro-pillars primarily showed shear banding along the critical resolved shear stress (CRSS) direction (Fig. 2e), whereas the pure crystalline micro-pillars showed multiple slip steps after deformation (Fig. 2f). The mixed micro-pillars showed a combination of the two behaviors mentioned in the previous lines.

The distribution of yield strengths (σ_v) for each phase as well as mixed pillars is shown in Fig. 3a. Engineering stress-strain plots for pillars on the crystalline dendrite and the amorphous matrix are shown in Fig. 3b. The glassy pillars showed on average a yield point of 1.91 GPa followed by serrated plastic deformation. Serrated flow accompanied by load drops in the stress-strain curve represents shear banding in the glassy matrix which has been widely reported for monolithic bulk metallic glasses [9]. Once a shear band nucleates and propagates during compression, the micro-pillar is plastically deformed and a corresponding load drop is seen in the stress-strain curve obtained in displacement controlled mode. The amplitude of the load drops was $\sim 0.5 \pm 0.2$ GPa. Almost all the pillars on the glassy phase showed comparable plastic deformation behavior with similar load drop frequency and amplitude. In contrast, the pillars on crystalline dendritic phase showed much lower yield strength, $\sigma_v \sim 0.72 \, \text{GPa}$. Micro-pillars on the crystalline dendrite were chosen in four different crystalline orientations and the average value of the yield strength is represented in Fig. 3a. The crystalline micro-pillars showed the lowest σ_v when the primary dislocation glide direction for the BCC dendrites, $\{110\}$ < - 111>, was parallel to the maximum resolved shear stress direction. After yielding, smooth plastic flow with no recognizable load burst was observed. All the crystalline pillars showed stable strainhardening after yield point and multiple slip steps with no catastrophic fracture was observed (Fig. 2f). The amorphous/crystalline mixed micro-pillars showed yield strength values in between those of the pure phases.

A number of pillars were FIB milled at the interface between the glassy matrix and crystalline dendrites. The engineering stress–strain plots of these micro-pillars are shown in Fig. 3c and d. As shown in Fig. 2c, one arrangement of mixed pillars contained the glassy matrix on top and dendritic phase on the bottom. Since the dendritic phase showed a lower σ_{ν} , yielding occurred first for the crystalline phase,



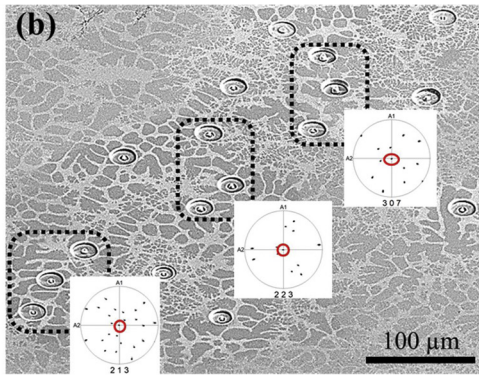


Fig. 1. (a) Electron backscatter diffraction IPF + IQ map of the BMGMC, showing the orientation of crystalline dendrites (colored), and the amorphous matrix shown in black; (b) SEM micrograph showing a region containing micro-pillars milled in the crystalline dendrites oriented along (213), (223), and (307) directions and pillars in the amorphous matrix of the BMGMC (insets show pole figures with a point in the center indicating the orientation of the micro-pillar).

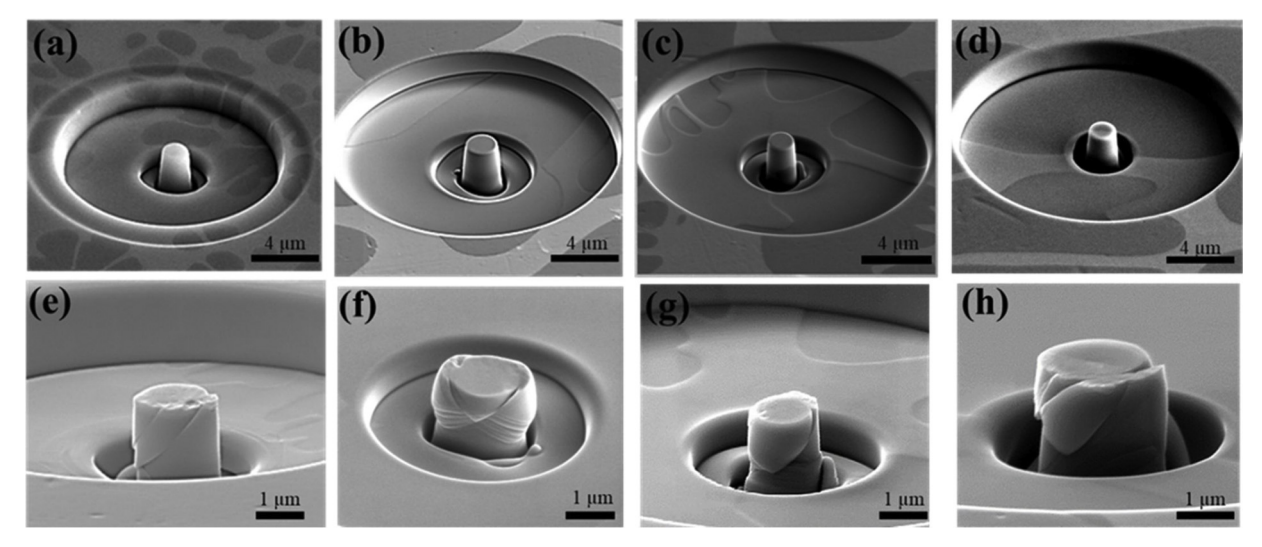


Fig. 2. SEM image of micro-pillars before deformation in (a) glassy matrix, (b) crystalline dendrite and (c and d) glass/dendrite interface; (e–h) Corresponding SEM images of the micro-pillars after uniaxial compression under quasi-static loading at a constant strain rate of $\sim 2.5 \times 10^{-4} \, \rm s^{-1}$.

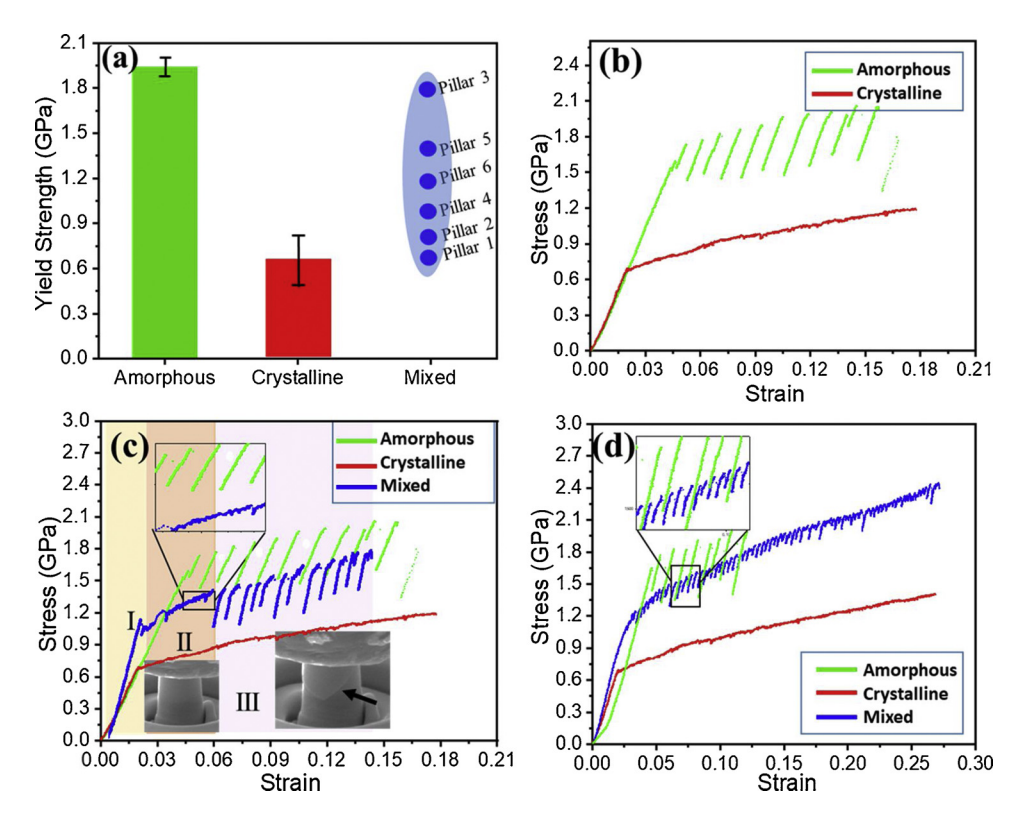


Fig. 3. (a) The average compressive yield strength (σ_y) of micro-pillars on amorphous matrix, crystalline dendrite and both phases (mixed pillars); (b) Uniaxial engineering stress–strain curves for the phase-specific micro-pillars – one entirely on the glassy matrix and another entirely on crystalline dendrite; (c) stress–strain curve of mixed pillar with glassy matrix on top and crystalline dendrite on the bottom; (d) stress–strain curve of mixed pillar with glassy mith the two phases side by side. The insets show *in situ* images in the plastic deformation region (see supplementary videos for details).

while the glassy section remains un-deformed (marked as region I in Fig. 3c) [10], acting as a rigid body. A load drop was observed right after the crystalline dendrite yielded followed by plastic deformation of the dendritic phase (region II in Fig. 3c). A second yielding related to the glassy matrix was observed once strain hardening in the dendritic phase approached the yield point of the amorphous matrix ~1.6 GPa [11]. At this point, multiple shear bands nucleated in the matrix, seen as load drops in the stress–strain plot (region III in Fig. 3c) [12]. Multiple yielding phenomenon has recently been reported for Cu–Zr–Al composites under compressive loading [13]. Large load drops after this transition showed that plastic flow continued primarily through deformation of the amorphous matrix since the amplitude and frequency of these bursts were identical to the pure glassy micro-pillars. The mixed pillars after deformation (Fig. 2g and 2 h) showed initially formed slip lines on the crystalline dendritic phase as well as

subsequent shear bands on the amorphous phase. The difference in plastic deformation behavior for each type of micro-pillar is evident from the $in\ situ$ videos of micro-pillar compression (supplementary videos). Slightly different mechanical response was observed when the crystalline dendrite and glassy sections were side by side in a micro-pillar. The calculated yield strength for this pillar was relatively higher and serrated plastic flow set in right after yielding (Fig. 3d). The σ_y value for this type of mixed micro-pillar was close to the yield strength of the pure amorphous matrix indicating that the external load in this case was carried by the amorphous matrix, while the presence of crystalline dendrite prevented catastrophic failure of the pillar and resulted in a more homogenous plastic flow. This arrangement of mixed micro-pillars demonstrated different plastic flow behavior, with higher frequency and lower amplitude of load drops, compared to pure amorphous pillars.

4. Discussion

The reported bulk tensile yield strength for the Ti-based BMGMC investigated in this study is $\sim 1.36\,\mathrm{GPa}$ [1], which is in between the yield strengths measured for the micro-pillars on the dendritic phase and the amorphous matrix. The composite consists of 53 vol% of glassy phase and 47 vol% of dendritic BCC phase [1]. The overall hardness and elastic modulus for a similar BMGMC was estimated by the rule of mixtures approach based on phase-specific measurements [14]. Using a similar methodology and average phase-specific strengths of the matrix (1.91 GPa) and crystalline dendrite (0.72 GPa), the overall value of σ_v was estimated to be ~1.35 GPa, which is very close to the reported value for the bulk strength measured from tensile testing. Insets in Fig. 3c and d show magnified views of the stress-strain plots where smooth plastic flow after yielding is clearly seen for the mixed pillars in contrast to the behavior of pure glassy pillars. For the vertical interface geometry of the mixed pillars in particular, the frequency of load drops was much higher while the amplitude was an order of magnitude lower compared to pure glassy pillars. Higher frequency and lower load drop amplitude as a function of pillar diameter has been reported for Zr₅₀Ti_{16.5}Cu₁₅Ni_{18.5} and Zr_{61.8}Cu₁₈Ni_{10.2}Al₁₀ metallic glasses, which was attributed to the size and density of isolated flow defects as the pillar diameter approached ~ 100 nm length-scale [15]. However, in the present study all the pillars had very similar dimensions and aspect ratios which ruled out the size effect of the pillars on their plastic deformation behavior. Smooth plastic flow in mixed pillars in contrast to pure glassy pillars may be attributed to reduced stored elastic energy [15-17]. The energy required for a shear band to traverse a pillar and lead to catastrophic failure comes from the stored elastic energy. The amount of required energy would not be sufficient for crack nucleation and propagation in case of pillars below a critical size, consequently leading to homogenous deformation [18]. Serrations on the stressstrain plots correspond to accumulation and release of elastic energy $(\Delta \delta)$, which may be determined as [19]:

$$\Delta \delta = \frac{1}{2} \Delta \sigma \frac{d^2}{4} \pi \varepsilon_e h,\tag{2}$$

where, $\Delta \sigma$ is the change in elastic stress, ε_e is the elastic strain limit (i.e. 0.02), and d and h are diameter and height of the micro-pillar, respectively. The released energy per unit area of shear band is defined by $\Delta\delta/A$, where A is the shear plane area defined as $A = \pi [d/2\sin\Theta]^2$, in which Θ is the angle between shear plane and loading axis. The average $\Delta\delta$ during a single load drop was calculated to be ~8.5 J m⁻² for pure amorphous micro-pillar, which is close to the value ($\sim 9 \, \mathrm{J \, m^{-2}}$) reported previously for a Zr-based BMG [20]. For mixed pillars, less elastic energy would be stored ($\Delta\delta \sim 2.5 \, \mathrm{J \, m^{-2}}$), as they showed more homogenous plastic flow during compression. Considering an analogy with Griffith criterion for crack propagation [18], a shear band would propagate only when the strain energy relief associated with the propagation exceeded the energy increment of the shear band. A critical value for the stored energy in the elastically strained volume of shear transformation zones (STZs) in a metallic glass is required below which homogenous plastic flow would prevail over shear banding [16]. In the case of mixed micro-pillars, there would be greater resistance towards shear band propagation due to the lower stored elastic energy. This may account for the higher fracture toughness seen in BMG composites compared to monolithic BMGs.

To further understand phase-specific response, high magnification post-deformation images of the micro-pillars were analyzed. The micro-pillar compression tests were stopped after certain degree of strain to capture the post-deformation images and better understanding of the deformation mechanism. Therefore, the total strain shown in the stress–strain curves of Fig. 3 does not represent the strain to failure for these micro-pillars. Fig. 4 shows the magnified views of the deformed pillars for the dendritic phase, amorphous matrix and the interface. Multiple slip bands were seen for the deformed micro-pillars containing

pure crystalline dendrites (Fig. 4a) while the pure glassy pillars predominantly demonstrated shear band formation (Fig. 4b). The wavy deformed features in crystalline micro-pillars may be related to crossslip of screw dislocations along <111> directions as commonly seen in BCC metals [21]. A combination of these features was seen for the mixed micro-pillars (Fig. 4c), where multiple slip lines were activated for the crystalline dendrite concurrent with discrete shear band formation for the glassy phase. In addition, shear band multiplication and branching was seen for the mixed micro-pillars (Fig. 4d). The primary shear band initiated at the top of the pillar was stretched into the crystalline dendrite and was constrained from further propagation. The interaction of multiple shear bands effectively eliminated localization of stress in the primary shear band and led to higher plasticity in case of the mixed pillar [14]. It has been shown that dislocation-mediated plastic flow in dendrite can accommodate plastic strain carried by shear bands in the amorphous matrix to conserve strain compatibility [22]. For the mixed micro-pillars, the interface may also aid in the initiation of shear bands once the yield point of the glass is exceeded. For the vertical interface geometry in particular, deformation may be dominated by nucleation of a large number of shear bands along the interface rather than propagation of a few dominant ones. This is supported by the stress-strain curve behavior seen in Fig. 3d, where serrations with higher frequency and smaller amplitude are seen for this geometry of the mixed pillar. In contrast, the fully amorphous micro-pillars showed lesser number of significantly larger load-drops. This behavior is also supported by the SEM images in Fig. 4, where large number of shear bands is seen in the mixed pillar (continuing from the slip lines on the crystalline phase, Fig. 4c) as opposed to few dominant shear bands for the fully amorphous pillar (Fig. 4b). The overall plastic deformation mechanism of pure and mixed phase micro-pillars is depicted schematically in Fig. 4e. In case of the mixed micro-pillars with side by side arrangement of the two phases, shear band propagation was arrested at the interface. In case of top down arrangement of the two phases. plastic deformation initiated on the crystalline dendrite in the form of slip lines and subsequently on the amorphous phase resulting in shear banding.

To understand deformation induced changes at the amorphous/ crystalline interface, high resolution transmission electron microscopy (HRTEM) was used for the deformed micro-pillars. Fig. 5a shows a FIB lift-out at the interface of crystalline dendrite (darker contrast) and amorphous matrix (bright contrast) in a mixed micro-pillar. A bright field image of the interface is shown in Fig. 5a1. High density of dislocations was seen in the dendritic region, which formed a series of parallel slip bands with a spacing of ~150 nm (Fig. 5b), very similar to the length-scales reported for Ti- and Zr-based BMG composites after deformation [11,23]. Furthermore, a series of secondary slip bands were observed at higher magnification inside each of these primary bands aligned at ~ 45° orientation with respect to the main slip bands, indicating the activation of multiple slip systems inside the BCC dendrite (Fig. 5b1). This may be attributed to the large plasticity accommodated by the crystalline phase during compression. High resolution TEM images with atomic arrangements at the glass/dendrite interface are shown in Fig. 5c-e. The zone axis for dendrite region was identified as [1 11] which revealed a disordered BCC crystal structure. The large amount of dislocation pile-up in the vicinity of dendrite/glass interface demonstrates significant accommodation of plastic deformation by the crystalline region. Inverse Fast Fourier Transition (IFFT) image containing atomic arrangement in the crystalline dendrite showed some degree of lattice distortion after plastic deformation (Fig. 5d). However, there was no indication of devitrification of the glassy matrix after plastic deformation (Fig. 5e). The corresponding selected area electron diffraction (SAED) patterns for each region are shown as insets.

Retardation of shear bands in crystalline dendrites has been recently reported for a Ti-based BMGMC at cryogenic temperatures [11]. Furthermore, formation of multiple shear bands instead of a single one suppresses catastrophic crack propagation and enhances plasticity and

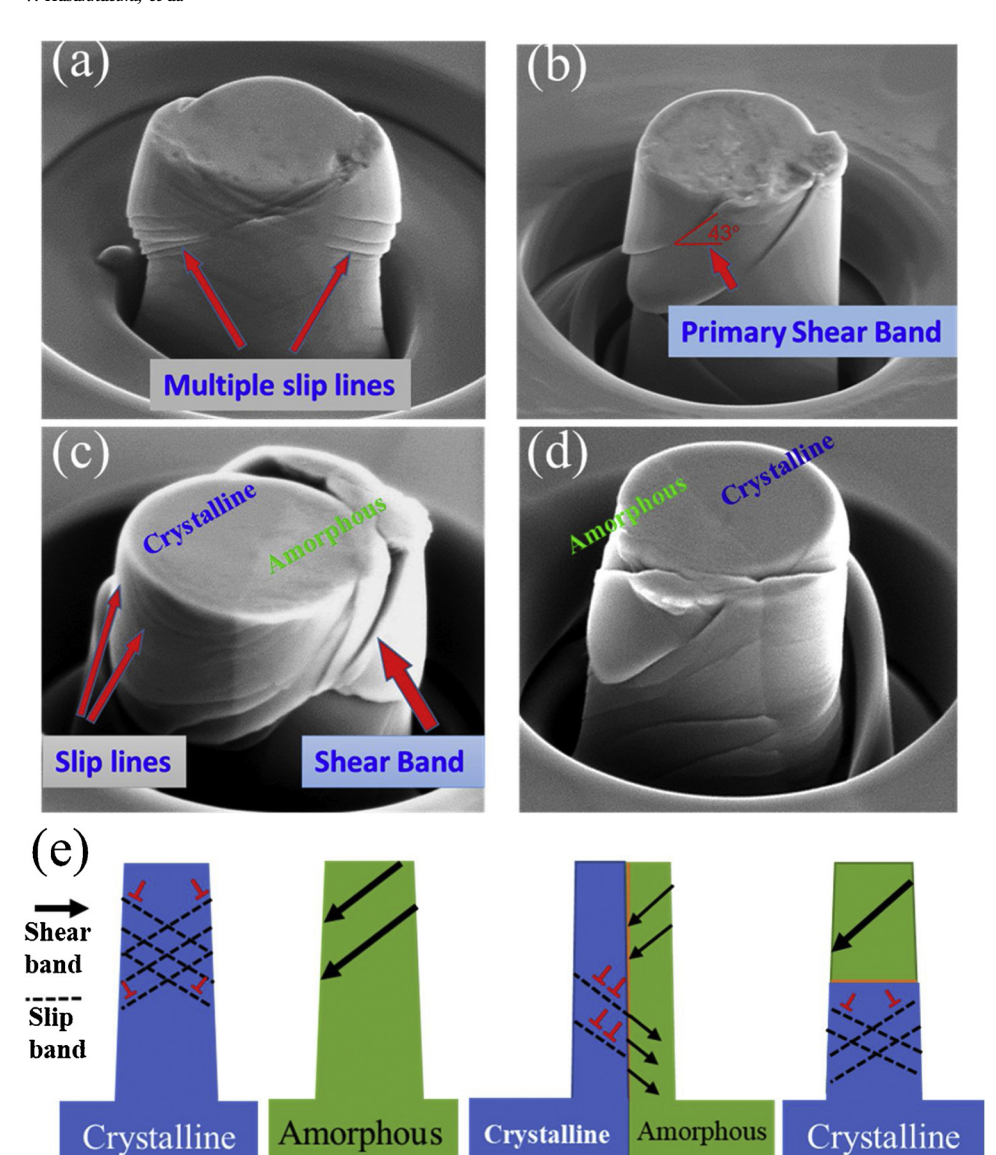


Fig. 4. (a) Micro-pillar in crystalline dendrite showing multiple slip bands on the surface; (b) micro-pillar in pure glassy matrix showing deformation along two primary shear bands; (c) front view of the mixed micro-pillar showing a combination of shear bands and slip bands; (d) back view of the same micro-pillar; (e) schematic showing slip and shear bands on the deformed crystalline and glassy micro-pillars, respectively. For side by side arrangement of the two phases, shear bands were arrested at the crystalline-amorphous interface. For top-down arrangement, yielding first occurred for the crystalline dendrite followed by shear banding in the glassy phase.

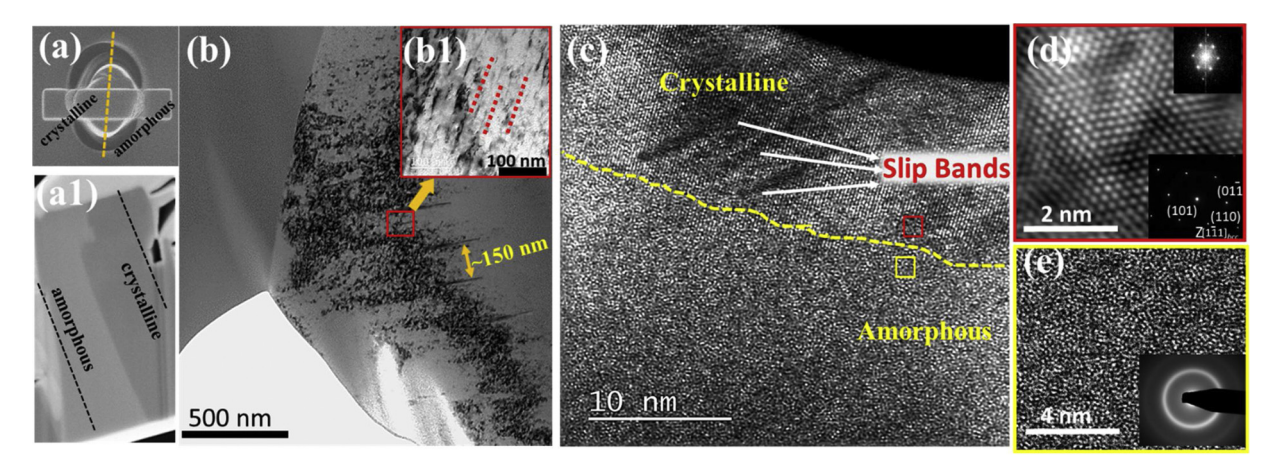


Fig. 5. FIB lift-out from the deformed mixed micro-pillar for TEM analysis: (a) top view and (a1) side view; (b) Bright-field TEM image of the glass/dendrite interface with the inset (b1) showing a series of secondary slip bands at a higher resolution; (c) HRTEM image of the interface between the dendrite and the glass; (d) HRTEM image of the deformed dendrite (red box in part c) with the insets showing the corresponding Inverse Fast Fourier transition (IFFT) image and SAED pattern; (e) HRTEM image of the glassy matrix (yellow box in part c) with the inset showing the corresponding SAED pattern.

toughness [7]. Multiplication of shear bands resulting in higher plasticity was clearly seen for the mixed micro-pillars in this study. Sluggish plastic deformation as a result of nanoscale networks of chemical heterogeneities has also been shown for Cu–Zr–Al–Y metallic glass [24]. Nucleation of multiple shear bands in the mixed pillars and their propagation in different directions might have resulted in accommodation of higher amount of strain before failure providing a pathway for design of composite materials with ultra-high toughness. Significant toughness enhancement, plasticity accommodation, and surface degradation resistance has been reported recently in the case of dual-phase eutectic high entropy alloys [25–27], dual-phase bimodal steels [28,29], and other multi-phase systems [30].

5. Conclusions

Site-specific mechanical response of an *in situ* Ti-based bulk metallic glass composite was investigated through uniaxial micro-pillar compression. Serrated plastic flow with large load drops was observed for the micro-pillars on the amorphous matrix, while smooth plastic deformation with much lower yield strength was seen for the pillars on crystalline dendrites. Homogeneous deformation and greater plasticity for the mixed micro-pillars was attributed to their smaller stored elastic energy. Shear bands initiated in the amorphous matrix were arrested by the crystalline dendritic phase, which accommodated plasticity through slip bands and dislocations pile-ups. The interface remained intact after plastic deformation, with no observable signs of devitrification in the amorphous phase.

CRediT authorship contribution statement

Vahid Hasannaeimi: Conceptualization, Methodology, Investigation, Writing - original draft, Writing - review & editing. Saideep Muskeri: Methodology, Investigation. Bharat Gwalani: Investigation. Douglas C. Hofmann: Validation, Writing - review & editing. Sundeep Mukherjee: Conceptualization, Supervision, Funding acquisition, Validation, Writing - review & editing.

Declaration of competing interest

The authors declare that they have no competing interests to influence the work reported in this paper.

Acknowledgements

This work was partly supported by funding from the National Science Foundation (NSF) under grant numbers 1561886, 1919220, and 1762545. Any opinions, findings, and conclusions expressed in this paper are those of the authors and do not necessarily reflect the views of the National Science Foundation (NSF). The authors also acknowledge the Materials Research Facility (MRF) and Advanced Materials and Manufacturing Processes Institute (AMMPI) at University of North Texas for the characterization facilities. DCH acknowledges financial support from the National Aeronautics and Space Administration (NASA) under contract no. NNH10ZTT001N.

Appendix A. Supplementary data

Supplementary material related to this article can be found, in the online version, at doi:https://doi.org/10.1016/j.mtcomm.2020. 101237.

References

[1] D.C. Hofmann, J.-Y. Suh, A. Wiest, M.-L. Lind, M.D. Demetriou, a.W.L. Johnson,

- Development of tough, low-density titanium-based bulk metallic glass matrix composites with tensile ductility, PNAS 108 (51) (2008) 20136–20140.
- [2] D.C. Hofmann, J. Suh, A. Wiest, G. Duan, M. Lind, M.D. Demetriou, W.L. Johnson, Designing metallic glass matrix composites with high toughness and tensile ductility, Nature 451 (2008) 1085–1090.
- [3] S.F. Guo, L. Liu, N. Li, Y. Li, Fe-based bulk metallic glass matrix composite with large plasticity, Scr. Mater. 62 (6) (2010) 329–332.
- [4] J.W. Qiao, S. Wang, Y. Zhang, P.K. Liaw, G.L. Chen, Large plasticity and tensile necking of Zr-based bulk-metallic-glass-matrix composites synthesized by the Bridgman solidification, Appl. Phys. Lett. 94 (2009) 151905-3.
- [5] J.R. Greer, J.T.D. Hosson, Plasticity in small-sized metallic systems: intrinsic versus extrinsic size effect, Prog. Mater. Sci. 56 (2011) 654–724.
- [6] Y. Wu, Y. Xiao, G. Chen, C.T. Liu, Z. Lu, Bulk metallic glass composites with transformation-mediated work-hardening and ductility, Adv. Mater. 22 (2010) 2770–2773
- [7] M.E. Launey, D.C. Hofmann, J.-Y. Suh, H. Kozachkov, W.L. Johnson, R.O. Ritchie, Fracture toughness and crack-resistance curve behavior in metallic glass-matrix composites, Appl. Phys. Lett. 94 (2009) 241910–241913.
- [8] E. Launey, D.C. Hofmann, W.L. Johnson, R.O. Ritchie, Solution to the problem of the poor cyclic fatigue resistance of bulk metallic glasses, PNAS 31 (2009) 4986–4991.
- [9] C.A. Schuh, T.C. Hufnagel, U. Ramamurty, Mechanical behavior of amorphous alloys, Acta Mater. 55 (12) (2007) 4067–4109.
- [10] J.W. Qiao, P.K. Liaw, Y. Zhang, Ductile-to-brittle transition of in situ dendrite-re-inforced metallic-glass-matrix composites, Scr. Mater. 64 (5) (2011) 462–465.
- [11] J. Bai, J.S. Li, J.W. Qiao, J. Wang, R. Feng, H.C. Ko, P.K. Liaw, Tensile deformation mechanisms of an in-situ Ti-based metallic glass matrix composite at cryogenic temperature, Sci. Rep. 6 (2016) 1–7.
- [12] J.W. Qiao, A.C. Sun, E.W. Huang, Y. Zhang, P.K. Liaw, C.P. Chuang, Tensile deformation micromechanisms for bulk metallic glass matrix composites: from work-hardening to softening, Acta Mater. 59 (2011) 4126–4137.
- [13] K.K. Song, S. Pauly, Y. Zhang, R. Li, S. Gorantla, N. Narayanan, U. Kühn, T. Gemming, J. Eckert, Triple yielding and deformation mechanisms in metastable Cu_{47.5}Zt_{47.5}Al₅ composites, Acta Mater. 60 (17) (2012) 6000–6012.
- [14] R.L. Narayan, K. Boopathy, Indrani Sen, D.C. Hofmann, U. Ramamurty, On the hardness and elastic modulus of bulk metallic glass matrix composites, Scr. Mater. 63 (2010) 768–771.
- [15] O. Kuzmin, Y. Pei, C. Chen, J.D. Hosson, Intrinsic and extrinsic size effects in the deformation of metallic glass nanopillars, Acta Mater. 60 (2012) 889–898.
- [16] O.V. Kuzmin, Y.T. Pei, J.T.M.D. Hossona, In situ compression study of taper-free metallic glass nanopillars, Appl. Phys. Lett. 98 (2011) 233104-3.
- [17] Y.Q. Cheng, E. Ma, Intrinsic shear strength of metallic glass, Acta Mater. 59 (4) (2011) 1800–1807
- [18] C.A. Volkert, A. Donohue, a.F. Spaepen, Effect of sample size on deformation in amorphous metals, J. Appl. Phys. 103 (2008) 083539-6.
- [19] F.H.D. Torre, A. Dubach, J. Schallibaum, J.F. Loffler, Shear striations and deformation kinetics in highly deformed Zr-based bulk metallic glasses, Acta Mater. 56 (2008) 4635–4646
- [20] A. Dubach, R. Raghavan, J. Loffler, J. Michler, U. Ramamurty, Micropillar compression studies on a bulk metallic glass in different structural states, Scr. Mater. 60 (2009) 567–570.
- [21] Y. Zou, S. Maiti, W. Steurer, R. Spolenak, Size-dependent plasticity in an Nb25Mo25Ta25W25 refractory high-entropy alloy, Acta Mater. 65 (2014) 85–97.
- [22] F. Szuecs, C.P. Kim, W.L. Johnson, Mechanical properties of Zr 56.2 Ti 13.8 Nb 5.0 Cu 6.9 Ni 5.6 Be 12.5 ductile phase reinforced bulk metallic glass composite, Acta Mater. 49 (2001) 1507–1513.
- [23] J.W. Qiao, Y. Zhang, P.K. Liaw, G.L. Chen, Micromechanisms of plastic deformation of a dendrite/Zr-based bulk-metallic-glass composite, Scr. Mater. 61 (2009) 1087–1090.
- [24] J. Kim, H.S. Oh, W. Kim, P.-P. Choi, D. Raabe, E.S. Park, Modulation of plastic flow in metallic glasses via nanoscale networks of chemical heterogeneities, Acta Mater. 140 (2017) 116–129.
- [25] S. Muskeri, V. Hasannaeimi, R. Salloom, M. Sadeghilaridjani, S. Mukherjee, Small-scale mechanical behavior of a eutectic high entropy alloy, Sci. Rep. 10 (2020) 2669.
- [26] V. Hasannaeimi, A.V. Ayyagari, S. Muskeri, R. Salloom, S. Mukherjee, Surface degradation mechanisms in a eutectic high entropy alloy at microstructural length-scales and correlation with phase-specific work function, Npj Mater. Degrad. 16 (2019) 1278.
- [27] V. Hasannaeimi, S. Mukherjee, Galvanic corrosion in a eutectic high entropy alloy, J. Electroanal. Chem. 848 (2019) 113331.
- [28] H.S. Arora, A. Ayyagari, J. Saini, K. Selvam, S. Riyadh, M. Pole, H.S. Grewal, S. Mukherjee, High tensile ductility and strength in dual-phase bimodal steel through stationary friction stir processing, Sci. Rep. 9 (2019) 1345.
- [29] R. Salloom, A.V. Ayyagari, S. Mukherjee, Nanoengineered hypereutectoid steel with superior hardness and wear resistance, J. Mater. Eng. Perform. 28 (2019) 2202–2211.
- [30] A. Ayyagari, V. Hasannaeimi, H. Arora, S. Mukherjee, Electrochemical and friction characteristics of metallic glass composites at the microstructural length-scales, Sci. Rep. 8 (2018) 906.